18

Rapid Kinetics

HISTORICAL BACKGROUND AND INTRODUCTION

After the concept of "steady state" was introduced to enzymology it became of interest, both from a theoretical and an experimental standpoint, to examine events during the course of the "pre-steady state". As the rate equations of many potential two- and three-substrate enzyme mechanisms were developed, it also became apparent that in a number of instances (see Chaps. 14 to 16) a mechanism could be tested by correlating a rate constant derived from steady-state kinetics with an experimentally determined rate constant. In these cases a rate constant for a binding step was usually involved.

Since many enzymes have turnover numbers on the order of 10^3 per second and higher, it is apparent that simple mixing and observation spectrophotometrically, in a manner suitable for the study of steady-state rates, is not sufficient for the examination of pre-steady-state phenomena or for the direct observation of binding phenomena, which in many instances are faster than the steady-state rate. This experimental limitation led to the development of a variety of rapid reaction techniques.

Initially, Hartridge and Roughton introduced the continuous-flow method for studying the combination of oxygen with hemoglobin. Two solutions, one containing oxygen, the other hemoglobin, were kept in elevated containers (see Fig. 18-1). From these, two tubes ran into a crude mixing chamber and then into an observation tube. To start the experiment the valves from the two containers were opened and the reactants allowed to mix and flow into the observation chamber. Spectrophotometric observations were made at various positions in the long observation chamber, representing (at a constant flow rate) different time intervals after mixing. Alter-

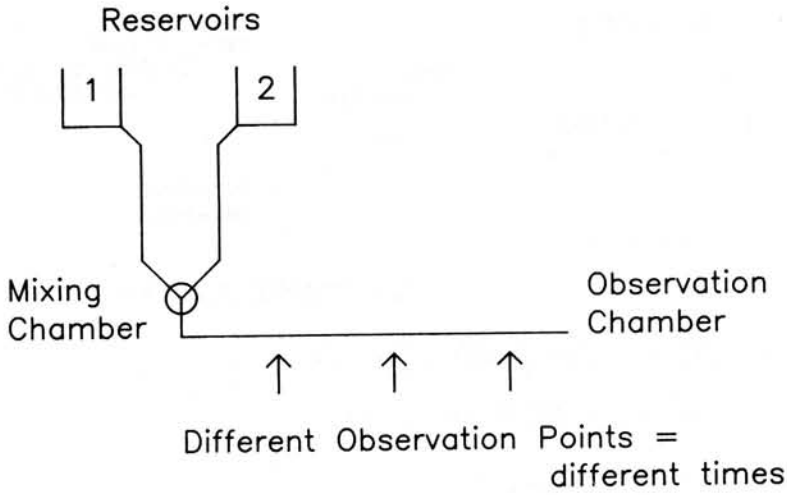

Figure 18-1 Outline of a continuous-flow method for following a rapid reaction.

natively, the pressure causing the flow could be changed, altering its velocity and allowing observations to be made at a fixed position. The time interval from mixing to the point of observation was determined (and if necessary altered) by the flow rate. Although this approach worked well, it used large amounts of material and had a relatively large "dead time" (which is the period of time between effective mixing and the start of observation).

This technique was later modified by Millikan, who used two syringes that could be coincidentally driven to deliver the reacting solutions to the mixing chamber and observation point. Chance further modified the approach, using an accelerated flow and a multijet mixing chamber. This, combined with the introduction of spectrophotometers, permitted dead times to be cut from several seconds to several milliseconds.

These developments led to the concept of "stopped" rather than continuous flow: In stopped flow the reactants are mixed and forced into an observation chamber and the flow stopped. The reacting mixture is then observed continuously as it ages. The main features of a stopped-flow rapid-mixing instrument are shown in Fig. 18-2, together with the way a stopped-flow experiment is usually performed. In many instances it is important to know the mixing, or premixing, order since premixing the enzyme with one or other of the reactants may alter the results observed or introduce experimental artifacts.

The major advantage of stopped flow is that very much smaller amounts of material are needed, and one continuously monitors the reaction rather than having to make a series of separate measurements at different time points. Since the mixing procedure is essentially the same as in the case of continuous flow, the dead time of a stopped flow experiment is of the order of 1 to 2 ms, depending on the exact design of the instrument. Modern stopped-flow instruments have pressure-driven syringes, permit observation of either fluorescence or absorbance, and have microprocessor control of data acquisition, allowing many replicates of the reaction to be rapidly collected and the data averaged and stored for later analysis.

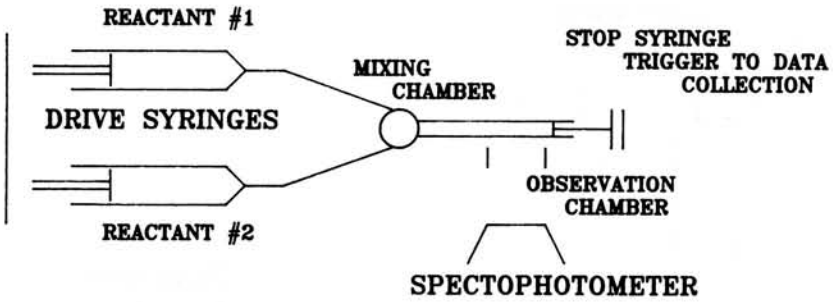

REACTION REPRESENTED AS:

ENZ + REACTANT #1

ENZ + REACTANT #2

Figure 18-2 Schematic representation of stopped-flow experiment. Reactions are usually indicated as shown.

The major limitation of such stopped-flow methodology resides in the dead time. As indicated, this is usually on the order of 1 to 2 ms. If, to collect sufficient data for accurate analysis we wish to observe 50% of the total reaction, the upper limit of the constant that can be estimated is obtained from the relationship for the half-time of the process, given by

$$t_{1/2} = \frac{0.693}{k} \tag{18-1}$$

If we use a dead time of 1 ms, the upper limit of the rate constant is approximately 700 μs^{-1}. In actual practice, for a single exponential process we need not follow 50% of the reaction and the practical upper limit is probably of the order of 1000 to 1500 s^{-1}. However, it is most important when only a small portion of the reaction is monitored that the *amplitude* of the process followed is consistent with the initial and final levels of product. If two exponential processes are occurring with well-separated rate constants and only the later stages of the slower process are followed, an examination of the amplitude of the followed process compared to the overall measured amplitude reveals the presence of a faster process occurring within the dead time of the method. This limitation of the dead time of a rapid-mixing approach led to the development of equilibrium perturbation techniques, which have dead times on the order of 5 to 10 μs. Such a dead time gives an upper limit for an observable rate constant of about 10^5 per second. Although some enzyme processes do occur at faster rates than this, most binding rates can be satisfactorily measured with this amount of dead time.

Before considering some of the early examples of rapid reaction studies (which illustrate the range of potential applications), we must consider several fundamental points.

1. In these experiments the enzyme is used in quantities whose stoichiometric relation to the substrate is not of the order used in initial rate experiments, and must be considered as a participant in the reaction rather than as a catalyst.

2. The concentration of substrate cannot be *assumed* to be constant in such experiments (although in certain types of experiments it may effectively be a constant).

3. For rapid reaction techniques to be applied, there must be some parameter that can be experimentally followed—usually in a continuous manner, although as we will see when considering some examples, this is not always necessary.

Early Examples of Rapid-Mixing Studies

Lipoyl Dehydrogenase. On reaction with a reducing substrate such as NADH, this enzyme undergoes a two-electron transfer that yields a compound with a long-wavelength absorbance. The second electron is probably transferred to a sulfur-containing group in the protein. Using rapid reaction techniques it was shown that in reactions with NADH using oxidized lipoic derivatives as electron acceptors, the rate-limiting step in each case is the reaction of the intermediate (with long-wavelength absorbance) with the oxidized lipoic acid derivative. The catalytically active intermediate does *not* give an ESR signal, presumably as a result of spin pairing between the flavin and the sulfur radical. The fully reduced form of the enzyme is formed by reaction with NADH, but its rate of oxidation by substrate is much slower than that of the intermediate, with the result that the overall reaction is inhibited. In most situations this is prevented because the fully reduced form is rapidly converted to the intermediate form by interaction with NAD.

D-Amino oxidase also forms intermediates with long-wavelength absorbance that must contain substrate since the shape of the spectrum depends on the type of amino acid substrate used. The intermediate is formed and removed at rates consistent with its participation in catalysis and is converted to a fully reduced form that appears slowly and is not involved in ordinary functioning; this form has no ESR spectrum.

A semiquinone form of enzyme results from reduction with dithionite and has an ESR spectrum but does *not* react with either oxygen or amino acids.

Glucose Oxidase. This enzyme functions by alternating between fully oxidized and reduced forms. However, no trace of a change in long-wavelength absorbance is observed. One can obtain a semiquinone form by reduction with dithionite, which gives an ESR spectrum, but it does *not* react readily with glucose or oxygen.

Microsomal NADP–Cytochrome c Reductase. This enzyme alternates between an intermediate and a fully reduced form. At the end of the reaction the enzyme remains in the intermediate form. On mixing oxidized enzyme with NADH, both the fully reduced and the intermediate forms appear together, which suggests that during reduction the two molecules of flavin (which are known to be associated with the enzyme) may cooperate, giving an electronic exchange formally equivalent to a

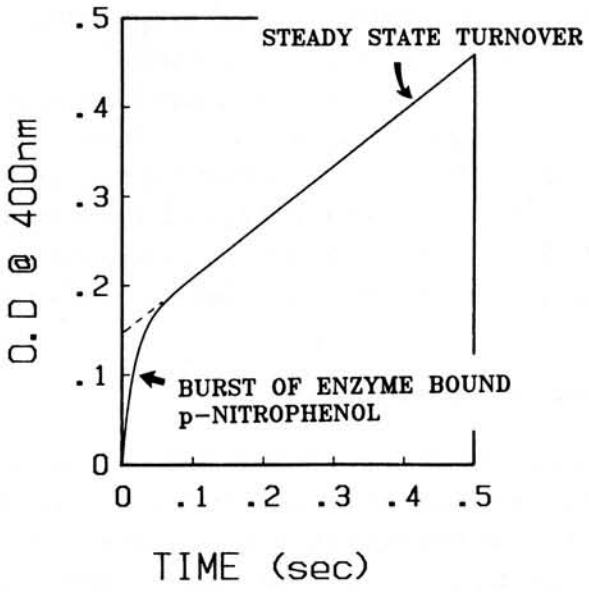

Figure 18-3 Outline of the experiment and experimental results obtained in stopped-flow experiments with trypsin and *p*-nitrophenyl acetate.

hydride-ion transfer, followed either by the full reduction of one flavin or by the appearance of an intermediate form of both flavins by intramolecular electron transfer.

Hydrolytic Enzymes. The reactions catalyzed by these enzymes are not associated with major spectrophotometric changes in enzyme and thus either the substrate or the product must be followed directly. Gutfreund followed the hydrolysis of *p*-nitrophenyl acetate, which gave a spectrophotometric change associated with hydrolysis that was markedly biphasic. The first phase was attributed to a relatively rapid formation of an enzyme–product complex, followed by slower turnover of enzyme as hydrolysis proceeded. This situation is illustrated in Fig. 18-3 and is important since it was one of the earliest demonstrations of a pre-steady-state "burst" of enzyme-bound product. We discuss the conditions that lead to the generation of a pre-steady-state "burst" of enzyme-bound product in more detail later in this chapter.

pH Changes. In reactions involving protons, Roughton and co-workers employed pH indicators to follow the rate of breakdown of carbonic acid in acid solution using a continuous-flow apparatus. Similar studies have been done to examine carbonic anhydrase and many other enzymes where a proton is involved.

Bioluminescent Reactions. Some bioluminescent systems require the simultaneous presence of several reactants before light emission takes place. Stopped-flow methods can give an indication of the order in which the various reactants enter the scheme. If three reactants are involved, one can use the various premixing steps shown in Fig. 18-4. If in the ordinary reaction the rate-limiting step is (b + c), and this reaction can take place in the absence of a, then on mixing (b + c) with a, light is observed much sooner than in the other premixing cases.

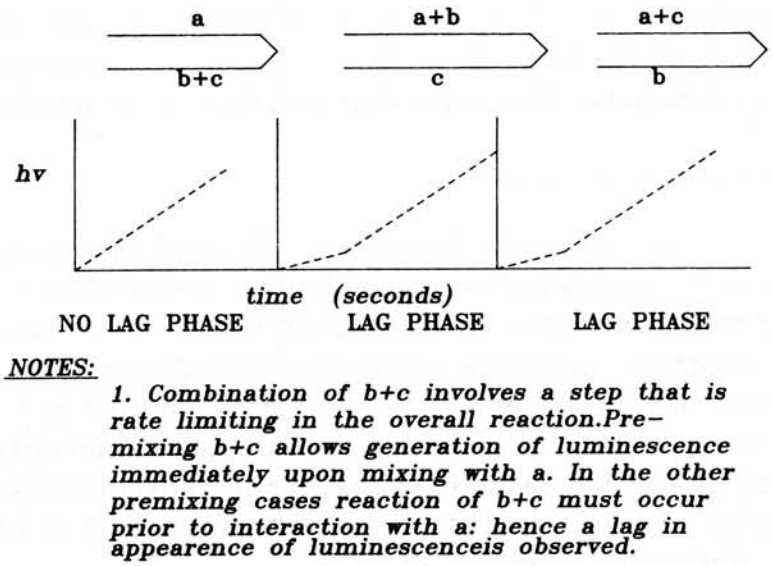

Figure 18-4 Premixing scheme for a reaction involving three reactants leading to the generation of bioluminescence.

Quenching Methods

In the general principle of quenching methods, two reactants are driven through a conventional mixer and along an observation tube that terminates in a second mixer fed with a quenching reagent, as outlined in Fig. 18-5. The rapid reaction is initiated on mixing and terminated on quenching, and the effluent is collected and analyzed later.

A variation is the rapid-freezing method. Reactants are mixed and sprayed into a large volume of isopentane at $-140°C$. Since fine jets are used, rapid freezing occurs. This method is used primarily in conjunction with ESR measurements. The dead time of the apparatus is made up of three components: the time for cooling from room temperature to 0°C, for freezing, and for cooling to $-140°C$. In addition,

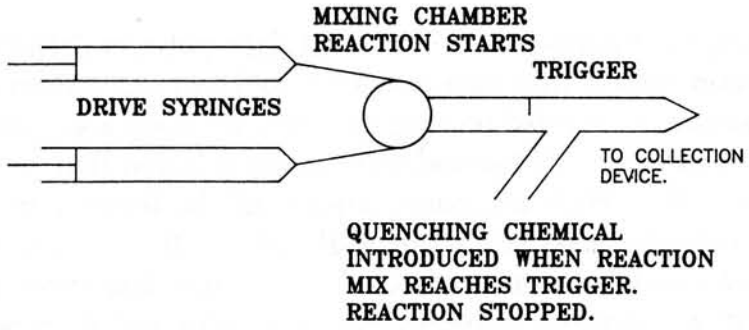

Figure 18-5 Scheme of the setup of a rapid-mix-and-quench experiment.

any reaction continuing at $-140°C$ must be taken into account, especially if long periods are left between the freezing and later analysis. This approach has been used successfully in studies on xanthine oxidase and on the copper in cytochrome oxidase.

Equilibrium Perturbation Methods

As indicated earlier, the major limitation with rapid mixing experiments is the dead time. To overcome this problem, equilibration perturbation methods were developed. The principle is simple: An equilibrium mixture is set up under a particular set of thermodynamic conditions, which are rapidly changed and the "relaxation" of the equilibrium mixture to the equilibrium defined by the new thermodynamic conditions monitored. Since no rapid mixing of reactants is involved, the approach is limited instead by the time taken to change the thermodynamic conditions of the equilibrium. In the two most used methods, temperature jump and flash photolysis, the change requires on the order of 1 to 10 μs.

Temperature Jump. This procedure consists of taking a solution at one temperature containing an enzyme and substrate at equilibrium, heating the solution as quickly as possible, and following the exchange between enzyme and substrate as the equilibrium readjusts itself to the new value corresponding to the new temperature.

The temperature jump is produced by an electrical discharge between electrodes placed in the solution, resulting in a temperature rise of about 5°C. In most cases the reaction is followed by absorbance spectrophotometry, although fluorescence recording has been used (care must be taken because of temperature dependence).

The time resolution is limited by the rate of the temperature jump. This is normally on the order of 10^{-5} s, which represents an improvement of two orders of magnitude over flow methods. Although it seems that temperature-jump methodology offers many advantages over rapid-mixing methods, there are a few disadvantages. It is applicable only to systems in which an equilibrium is obtained with a reasonable amount of ligand present free in solution, and with an equilibrium that is perturbable. Also, there is the technical difficulty in producing a vigorous electric discharge in close proximity to a sensitive detection system.

Flash Photolysis. Energy, in the form of a light pulse, is delivered to the system under examination with a time constant of 5 to 10 μs for a flash energy of about 1000 J. The reaction is recorded photographically by using a second flash tube—the "spectroflash"—which records the spectrum of the solution that is being illuminated with the "photoflash." With electronic control of the interval between the photo and spectro flashes, the time resolution is about 1×10^{-5} s. Flash photolysis has many applications, including the study of the formation and spectra of triplet forms of chlorophyll in nonaqueous solvents, the formation and disappearance of long-wavelength absorbance derived from FMN coenzymes, and the interactions of heme-containing proteins with carbon monoxide. In hemoglobin and cytochrome oxidase, interactions with CO_2 were followed and it was found that the rate of reaction was about 60 times faster than had been determined by stopped-flow methods.

ASSOCIATION AND DISSOCIATION RATE CONSTANTS

A number of types of reactions illustrate the development of the theoretical basis for various rapid reaction techniques.

Simple Reactions

First examine a reactant, A, going to product, P, with a rate constant, k_1, and with the rate of the reaction given by

$$\frac{d\mathrm{A}}{dt} = -k_1\mathrm{A} \tag{18-2}$$

Integration of Eq. (18-2) yields

$$\mathrm{A}_t = \mathrm{A}_0 e^{-k_1 t} \tag{18-3}$$

where A_0 is the initial concentration of A and A_t is the concentration at time $= t$. If the product P is followed, then, since $\mathrm{A}_t + \mathrm{P}_t = \mathrm{A}_0$, we get

$$\mathrm{P}_t = \mathrm{A}_0(1 - e^{-k_1 t}) \tag{18-4}$$

The *half-time* of the reaction, $t_{1/2}$, where $\mathrm{A} = \mathrm{P} = \mathrm{A}_0/2$, is given by substitution into Eq. (18-1), and we define a new parameter, τ, where $\tau = 1/k_1 = 1/k_{\mathrm{obs}}$.

Reversible Reactions

If product P can react, with a rate constant k_2, to give A, we have a reversible reaction,

$$\mathrm{A} \underset{k_2}{\overset{k_1}{\rightleftharpoons}} \mathrm{P}$$

and can define an equilibrium constant K_e by

$$K_e = \frac{[\mathrm{P}]}{[\mathrm{A}]} = \frac{k_1}{k_2} \tag{18-5}$$

In this case $d\mathrm{A}/dt = -k_1[\mathrm{A}] + k_2[\mathrm{P}]$, but since $\mathrm{A}_t + \mathrm{P}_t = \mathrm{A}_0$,

$$\frac{d\mathrm{A}}{dt} = -k_1[\mathrm{A}] + k_2([\mathrm{A}_0] - [\mathrm{A}]) \tag{18-6}$$

This equation is integrated by separating the variables and multiplying each side by an exponential factor to give

$$\frac{d\mathrm{A}}{dt} + [\mathrm{A}](k_1 + k_2) = k_2\mathrm{A}_0 \tag{18-7}$$

$$\frac{d\mathrm{A}}{dt} e^{k_1 + k_2} + [\mathrm{A}](k_1 + k_2)e^{(k_1 + k_2)t} = k_2[\mathrm{A}_0]e^{(k_1 + k_2)t} \tag{18-8}$$

Therefore,

$$\frac{d}{dt([\mathrm{A}]\, e^{(k_1+k_2)t})} = k_2[\mathrm{A}_0]e^{(k_1+k_2)t} \tag{18-9}$$

and

$$[\mathrm{A}]e^{(k_1+k_2)t} = \frac{k_2}{k_1+k_2}[\mathrm{A}]e^{(k_1+k_2)t} + C \tag{18-10}$$

where C is a constant. However, boundary conditions apply: namely, that at $t = 0$, $\mathrm{A} = \mathrm{A}_0$, and that at $t =$ infinity, the equilibrium concentration of A, $\mathrm{A}_{eq} = \mathrm{A}_0 k_2/(k_1 + k_2)$. Therefore,

$$\mathrm{A}_t = \frac{\mathrm{A}_0}{k_1+k_2}[k_1 e^{-(k_1+k_2)t} + k_2] \tag{18-11}$$

This expression can be divided into two terms: the exponential term with rate constant (k_{obs}), where in terms of relaxation kinetics, $k_{obs} = 1/\tau = k_1 + k_2$, and an amplitude factor, given by $k_1/(k_1 + k_2)$.

Two important points: (1) the measured rate constant for the approach to equilibrium is a simple exponential and is greater than either of the individual first-order rate constants—in fact, $1/\tau = k_1 + k_2$; and (2) k_1 and k_2 cannot be determined without a knowledge of the amplitude factor—however, if the concentrations of A and P at equilibrium are known, k_1 and k_2 can be estimated.

Enzyme–Substrate Association. If we consider the reaction $\mathrm{E} + \mathrm{A} \rightleftharpoons \mathrm{EA}$, then if $\mathrm{A} \gg \mathrm{E}$, the reaction is effectively first order, and the system reduces to

$$\mathrm{E} \underset{k_2}{\overset{k_1\mathrm{A}}{\rightleftharpoons}} \mathrm{EA}$$

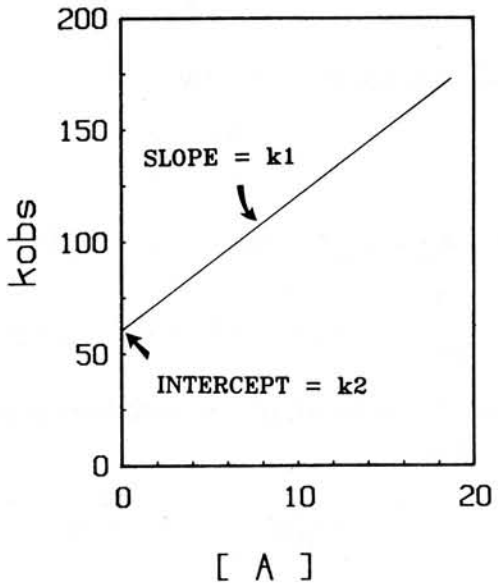

Figure 18-6 Dependence of k_{obs} on [A] for an enzyme–ligand association–dissociation reaction.

By analogy with the previous discussion, the relaxation time for this reaction is

$$\frac{1}{\tau} = k_2 + k_1 A = k_{obs} \tag{18-12}$$

Since the rate constants are pseudo-unimolecular there is a concentration dependence of k_{obs}. Thus k_1 and k_2 can be obtained *without* the amplitude factor by following the dependence of k_{obs} on [A] as illustrated in Fig. 18-6.

Displacement Experiments. Consider the experimental situation shown in Fig. 18-7. A′ is a displacing ligand present in excess such that its rate of binding is effec-

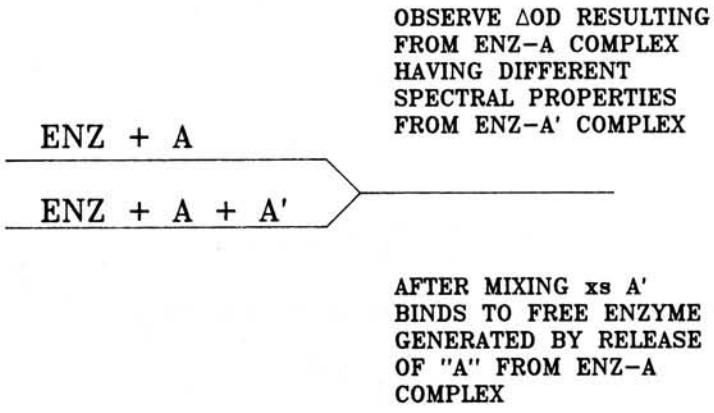

Figure 18-7 Scheme for a ligand displacement experiment.

tively infinitely fast and irreversible. The situation becomes, in effect,

$$A' + EA \xrightarrow{k_2} EA' + A$$

and resembles the simple irreversible reaction considered first. Thus $k_{obs} = k_2$, the off-velocity constant for A from the EA complex, and the analysis is quite simple.

Thermodynamic Principles of Relaxation

For a particular reaction the equilibrium concentrations of the reactants are dependent on some thermodynamic variable such as temperature.

Considering our earlier example, E + A → EA, the equilibrium constant K can be written

$$K = \frac{(\bar{E})(\bar{A})}{\overline{EA}} = e^{-\Delta H^\circ/RT} + e^{\Delta S^\circ/R} \tag{18-13}$$

where $\bar{E}$, $\bar{A}$, and $\overline{EA}$ are the equilibrium concentrations and ΔH° and ΔS° are the standard enthalpy and entropy changes for the reaction. To consider the effects of temperature, we must differentiate the expression for ln K, to give

$$d(\ln K) = (\bar{E}^{-1}\, d\bar{E}) + (\bar{A}^{-1}\, d\bar{A}) - (EA^{-1}\, d\overline{EA}) \tag{18-14}$$

But since $d\mathrm{EA} = -d\bar{\mathrm{E}} = -d\bar{\mathrm{A}}$, we get

$$d(\ln k) = (\bar{\mathrm{E}}^{-1} + \bar{S}^{-1} + \overline{\mathrm{EA}}^{-1})\, d\bar{\mathrm{E}} \tag{18-15}$$

From the van't Hoff relationship,

$$d(\ln K) = \frac{\Delta H^\circ}{RT^2}\, dT \tag{18-16}$$

Thus

$$d\mathrm{E} = \frac{1}{\bar{\mathrm{E}}^{-1} + \bar{\mathrm{A}}^{-1} + \overline{\mathrm{EA}}^{-1}} \frac{\Delta H^\circ}{RT^2}\, dT \tag{18-17}$$

and

$$d\mathrm{E} = \Gamma \frac{\Delta H^\circ}{RT^2}\, dT \tag{18-18}$$

where

$$\Gamma = \frac{1}{\bar{\mathrm{E}}^{-1} + \bar{\mathrm{A}}^{-1} + \overline{\mathrm{EA}}^{-1}}$$

Therefore, for a definite change in temperature, ΔT, we get

$$\Delta\bar{\mathrm{E}} = \Gamma \frac{\Delta H^\circ}{RT^2}\, \Delta T \tag{18-19}$$

Similarly, we can obtain expressions for the equilibrium shifts in $\bar{\mathrm{A}}$ and $\overline{\mathrm{EA}}$ from the expression

$$\Delta\bar{\mathrm{E}} = \Delta\bar{\mathrm{A}} = -\Delta\overline{\mathrm{EA}} \tag{18-20}$$

From Eq. (18-19) it is readily apparent that the perturbation of the equilibrium is dependent on two parameters: the equilibrium position itself, as expressed by Γ, and ΔH°.

If we consider the reaction

$$\mathrm{E} + \mathrm{A} \underset{k_2}{\overset{k_1}{\rightleftharpoons}} \mathrm{EA}$$

at equilibrium, when the system is suddenly heated, the concentrations [E], [A], and [EA], defined by the old equilibrium, are no longer the equilibrium concentrations of the new equilibrium, which may be symbolized by $[\bar{\mathrm{E}}]$, $[\bar{\mathrm{A}}]$, and $[\overline{\mathrm{EA}}]$, and

$$\frac{d[\mathrm{EA}]}{dt} = (k_1[\mathrm{E}][\mathrm{A}]) - (k_2[\mathrm{EA}]) \tag{18-21}$$

Equation (18-21) may be rewritten

$$\frac{d([\overline{\mathrm{EA}}] + \Delta[\mathrm{EA}])}{dt} = k_1([\bar{\mathrm{E}}] + \Delta[\mathrm{E}])([\bar{\mathrm{A}}] + \Delta[\mathrm{A}]) - k_2([\overline{\mathrm{EA}}] + \Delta[\mathrm{EA}]) \tag{18-22}$$

$$\frac{d[\overline{EA}]}{dt} + \frac{d\,\Delta[EA]}{dt} = k_1[\bar{E}][\bar{A}] + k_1([\bar{A}]\,\Delta[E] + [\bar{E}]\,\Delta[A]) + k_1\,\Delta[E]\,\Delta[A] - k_2[\overline{EA}] + k_2\,\Delta[EA] \quad (18\text{-}23)$$

From the equilibrium condition

$$\frac{d[\overline{EA}]}{dt} = k_1[\bar{E}][\bar{A}] - k_2[\overline{EA}] = 0 \quad (18\text{-}24)$$

Hence

$$d\,\Delta[EA] = k_1([\bar{A}]\,\Delta[E] + [\bar{E}]\,\Delta[A]) + k_1\,\Delta[E]\,\Delta[A] + k_2\,\Delta[EA] \quad (18\text{-}25)$$

If $\Delta[E], \Delta[A] \ll [E]$ and $[A]$, we get

$$\frac{d\,\Delta[EA]}{dt} = k_1([\bar{A}]\,\Delta[E] + [\bar{E}]\,\Delta[A]) - k_2\,\Delta[EA] \quad (18\text{-}26)$$

Adding the conditions $\Delta[E] = \Delta[A]$, and $\Delta[A] + \Delta[EA] = 0$, Eq. (18-26) becomes

$$\frac{d\,\Delta[EA]}{dt} = -(k_1([\bar{E}] + [\bar{A}]) + k_2)\,\Delta[EA] \quad (18\text{-}27)$$

which yields

$$\Delta[EA] = \Delta[EA]^\circ e^{-(k_1([\bar{E}]+[\bar{A}])+k_2)t} = \Delta[EA]^\circ e^{-1/\tau} \quad (18\text{-}28)$$

From these final equations, it is quite apparent that k_{obs} $(= 1/\tau)$ is equal to $k_1[\bar{E} + \bar{A}] + k_2$, and hence a plot of k_{obs} versus $[\bar{E} + \bar{A}]$ is linear, as shown in Fig. 18-8.

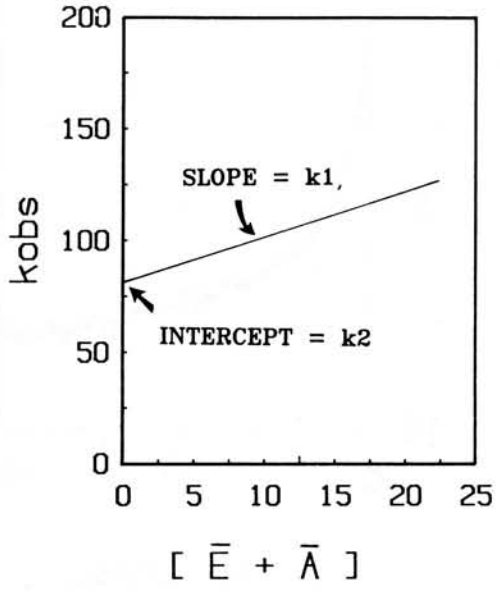

Figure 18-8 Dependence of k_{obs} on $[E + A]$.

So far we have examined a situation where an equilibrium is perturbed by a temperature change; however, the mathematical analysis is independent of *how* the perturbation is produced. In fact, one can combine the stopped-flow technique with the relaxation analysis and perform a "concentration-jump" experiment: the enzyme and ligand are preequilibrated in one syringe and then rapidly mixed with buffer plus any coligands contained in the other syringe. The decrease in spectral signal is monitored as the new equilibrium concentrations are established.

The concentration-jump technique is useful only if the equilibrium position is not too far to one side; otherwise, reequilibration upon dilution results in immeasurable concentration changes. Perturbation, in any case, results in relatively small concentration changes even with a favorable equilibrium. The analysis of the data obtained in such a concentration-jump experiment is identical to that used in a temperature-jump experiment.

In such an experiment, however, there are problems that may arise from the deliberate change in protein concentration. This is especially true in cases where the protein may undergo a concentration-dependent polymerization reaction. As in a regular stopped-flow experiment, this could contribute to the observed signal. Control experiments, where enzyme alone is subjected to the concentration jump, indicate such problems and provide "blank" reactions that can be subtracted from the experimental data in the presence of ligand. The case of glutamate dehydrogenase, which undergoes a concentration-dependent polymerization, illustrates this problem. Binding of the coenzyme NADPH can be followed by fluorescence changes, and data obtained in a typical concentration-jump experiment are given in Fig. 18-9.

Fluorescence is monitored as a function of time as enzyme–NADPH complex is subjected to rapid dilution. The continuous line shows the fit to an equation for two exponentials. When the experiment is repeated in the absence of coenzyme, one

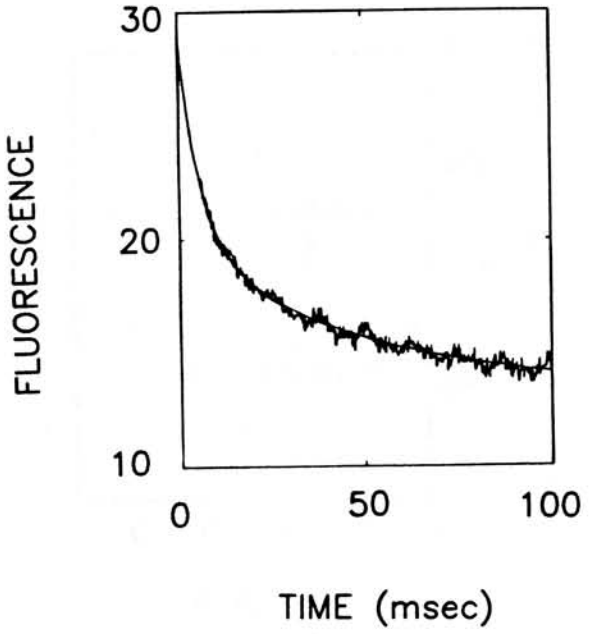

Figure 18-9 Fluorescence changes obtained in a concentration-jump experiment with glutamate dehydrogenase.

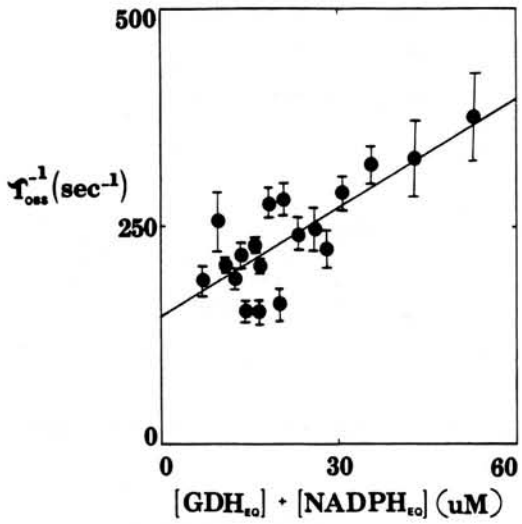

Figure 18-10 Relaxation times obtained from concentration-jump experiments. The bars represent estimated standard errors obtained from the fit. The straight line is a linear least-squares fit of the data.

of the exponentials is obtained, and is due to fluorescence intensity changes resulting from the depolymerization reaction of the enzyme as its concentration is decreased. The observed relaxation time for the other exponential is plotted (as its reciprocal) versus the calculated equilibrium concentrations of (enzyme + NADPH) in Fig. 18-10. Values for the association rate and the dissociation rate constant are obtained from the slope and intercept, respectively.

CATALYTIC TURNOVER EXPERIMENTS

So far we have considered ways to determine rate constants experimentally for the association and dissociation of ligand bound to enzyme. Rapid reaction techniques have also been applied to the analysis of enzymes undergoing catalytic reaction. Under conditions where the complete reaction is possible, rapid reaction techniques have the capability of examining various facets of the pre-steady-state phase. A variety of experiments are possible. If we consider the case where product formation is being monitored we observe a "pre-steady-state" phase only under conditions where product release is the overall rate-limiting step in the reaction cycle. This immediately gives information about the kinetic mechanism of the enzyme—it cannot obey a simple rapid-equilibrium random-order kinetic mechanism. If it did, no pre-steady-state phase could be observed in such an experiment: Product formation is the overall rate-limiting step. In situations where a pre-steady-state phase of the overall reaction is observed, however, we can examine a number of interesting questions.

Spectral Characterization of the Pre-Steady State

Some idea of the number and chemical nature of intermediates that contain product can be gotten from spectral studies on the pre-steady-state phase of the reaction. Such studies are performed by acquiring data over a period of, for example

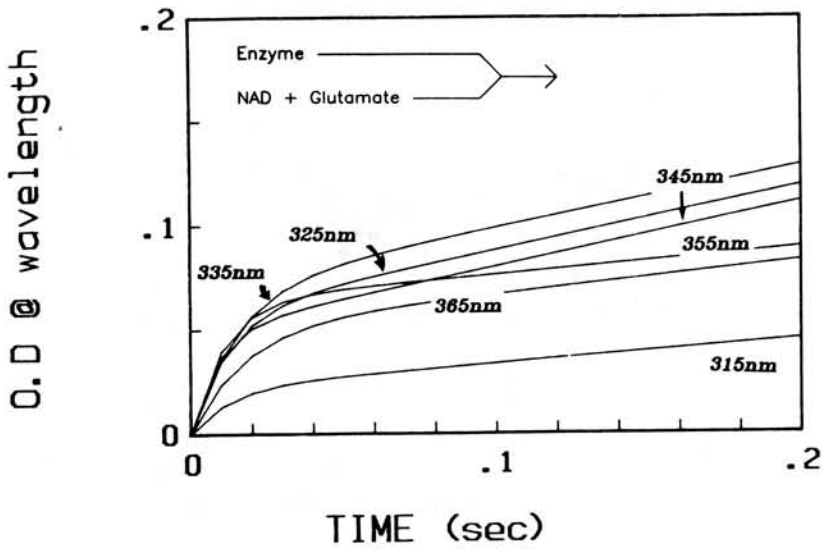

Figure 18-11 Stopped-flow traces obtained at the indicated observation wavelengths for the reaction shown in the inset.

1 s, at a series of different wavelengths covering the potentially interesting range. Although somewhat tedious, it is usually reasonable to obtain data at intervals of 2.5 to 5 nm over a 50 to 100 nm range. From the accumulated data, spectra can be constructed at whatever time intervals are desired. The data are usually represented as "time-difference" spectra, using two different time points in the reaction. Such spectra allow spectral characterization of species formed between the two time points. For example, if glutamate dehydrogenase is rapidly mixed with NAD and glutamate at pH 8.0, a pre-steady-state burst is observed when the reduced coenzyme product is monitored by absorbance measurements. This indicates that a product release step is rate limiting in the overall reaction. When a series of identical reactions are performed using different wavelengths of observation, a series of traces are obtained, as shown in Fig. 18-11. From such data, time-difference spectra can be calculated.

Typical results are given in Fig. 18-12, where the spectra are calculated from the points indicated by the arrows in Fig. 18-11. In this particular case a clear "blue-shifted" species is observed at 25 ms into the burst phase of the reaction. This species shifts to a "red-shifted" spectrum (curve 2) at approximately 100 ms, before finally resolving into the unshifted spectrum of free NADH (curve 3) at the end of the burst phase. For clarity it is convenient to present the data in the manner shown here, as this avoids multicomponent spectra that would be hard to interpret.

Derivation of Equations for Burst Amplitude and Analysis of Rate Constants

Apart from the spectral characterization of transients occurring in the pre-steady-state phase of a reaction, two other parameters can be measured in addition to the steady-state rate. These are the "burst" size and rate. The burst size is usually ob-

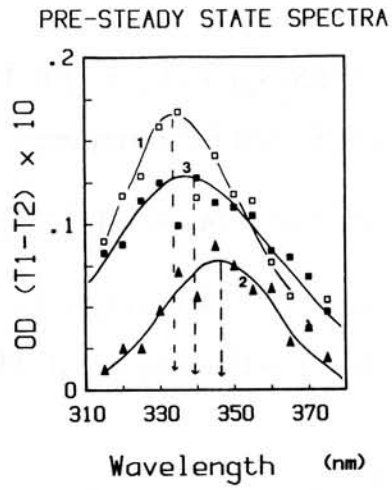

Figure 18-12 Time-difference spectra obtained from the data shown in Fig. 18-11; curve 1, $T_1 = 25$ ms, $T_2 = 0.5$ ms; curve 2, $T_1 = 100$ ms, $T_2 = 35$ ms; curve 3, $T_1 = 200$ ms, $T_2 = 100$ ms.

tained by extrapolation of the steady state to $t = 0$, as in Fig. 18-13, while the burst rate is the rate of the exponential process leading to the steady-state region. For the reaction

$$E + S_1 + S_2 \rightleftharpoons ES_1S_2 \rightleftharpoons EP_1P_2 \rightleftharpoons E + P_1 + P_2$$

under V_{max} conditions (i.e., when $[S_1] \rightarrow$ infinity and $[S_2] \rightarrow$ infinity), the simplest model for the formation of products can be written as

$$ES_1S_2 \underset{k_2}{\overset{k_1}{\rightleftharpoons}} EP_1P_2 \xrightarrow{k_3} E + P_1 + P_2$$

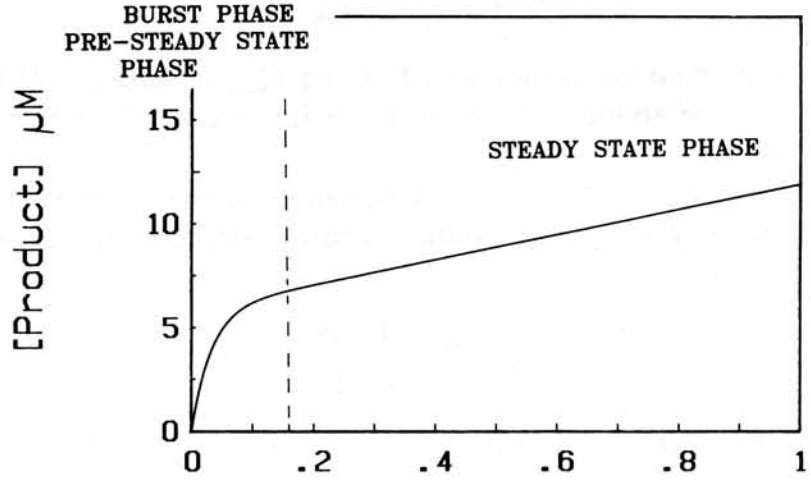

Figure 18-13 Phases of an enzyme reaction observed in a typical stopped-flow experiment.

and the total enzyme concentration

$$\mathrm{ET} = [\mathrm{ES_1S_2}] + [\mathrm{E}] + [\mathrm{EP_1P_2}]$$

Hence using $\mathrm{E_S}$ to represent $\mathrm{ES_1S_2}$ and EP to represent $\mathrm{EP_1P_2}$, we write

$$\frac{d(\mathrm{EP})}{dt} = k_1[\mathrm{ES}] - (k_2 + k_3) \cdot [\mathrm{EP}] \tag{18-29}$$

$$= k_1[\mathrm{ET} - \mathrm{EP}] - (k_2 + k_3) \cdot [\mathrm{EP}] \tag{18-30}$$

$$= k_1\mathrm{ET} - (k_1 + k_2 + k_3) \cdot [\mathrm{EP}] \tag{18-31}$$

Therefore,

$$\frac{d[\mathrm{EP}]}{dt} + (k_1 + k_2 + k_3)[\mathrm{EP}] = k_1\mathrm{ET} \tag{18-32}$$

and the concentration of EP is given by

$$[\mathrm{EP}] = \frac{k_1\mathrm{ET}}{k_1 + k_2 + k_3} + Be^{-(k_1 + k_2 + k_3)t} \tag{18-33}$$

when $t = 0$, $[\mathrm{EP}] = 0$, and

$$B = \frac{-k_1\mathrm{ET}}{k_1 + k_2 + k_3}$$

Therefore,

$$[\mathrm{EP}] = \frac{k_1\mathrm{ET}}{k_1 + k_2 + k_3}(1 - e^{-(k_1 + k_2 + k_3)t}) \tag{18-34}$$

when t approaches infinity,

$$[\mathrm{EP}] = \frac{k_1\mathrm{ET}}{k_1 + k_2 + k_3}$$

and is the steady-state concentration of EP under $V_{\max}$ conditions. If $k_1 \gg k_2 + k_3$, then EP = ET and the amount of EP is approximately equal to the total enzyme active-site concentration.

Similarly, from the formal mechanism we can write an expression for the formation of free product P, which is the product whose concentration can be monitored. $d\mathrm{P}/dt = k_3[\mathrm{EP}]$, hence

$$[\mathrm{EP}] = \frac{1}{k_3}\frac{d\mathrm{P}}{dt} \tag{18-35}$$

From Eqs. (18-33) and (18-35) we get

$$\frac{d[\mathrm{EP}]}{dt} = \frac{1}{k_3}\frac{d^2\mathrm{P}}{dt^2} = [k_1\mathrm{ET} - (k_1 + k_2 + k_3)]\frac{1}{k_3}\frac{d\mathrm{P}}{dt} \tag{18-36}$$

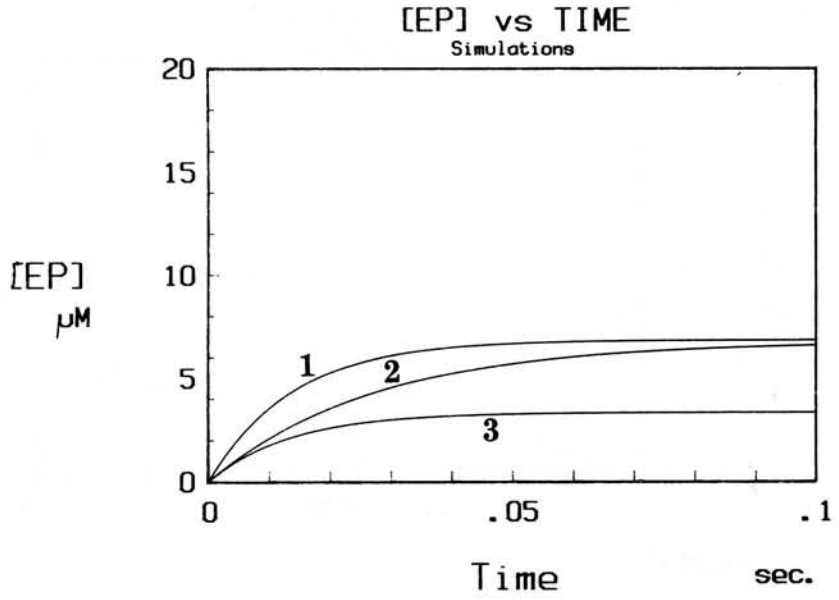

Figure 18-14 Computer simulations of [EP] versus time curves. k_1 is the rate constant for ES → EP, k_2 is the rate constant for EP → ES, and k_3 is the rate constant for product release, EP → E + P.

Constant	*Curve 1*	*Curve 2*	*Curve 3*
k_1	50	25	25
k_2	20	10	25
k_3	3	2	25

Hence

$$\frac{d^2\mathrm{P}}{dt^2} + (k_1 + k_2 + k_3)\frac{d\mathrm{P}}{dt} = k_1 k_3 \mathrm{ET} \tag{18-37}$$

Therefore

$$[\mathrm{P}] = \frac{k_1 k_3 \mathrm{ET}}{k_1 + k_2 + k_3}\, t - \frac{k_1 k_3 \mathrm{ET}}{(k_1 + k_2 + k_3)^2}\left(1 - e^{-(k_1 + k_2 + k_3)t}\right) \tag{18-38}$$

Figures 18-14 and 18-15 show the dependence of the formation of EP or P on t, as described by Eqs. (18-34) and (18-38), respectively. When t is large, the exponential term is negligible and a linear P versus t plot results, with

$$\text{slope} = \frac{k_1 k_3 \mathrm{ET}}{k_1 + k_2 + k_3}$$

which is equal to V_{max} by steady-state treatment of the mechanism.

From these simulations it is apparent (Fig. 18-14) that k_2 has a major effect on the rate of attainment of the steady-state concentration of EP, and that the steady-state concentration of EP is markedly affected by the relative rate of k_3. Under the various conditions in Fig. 18-14, the steady-state concentration of EP is *not* stoichiometric with the active-site concentration.

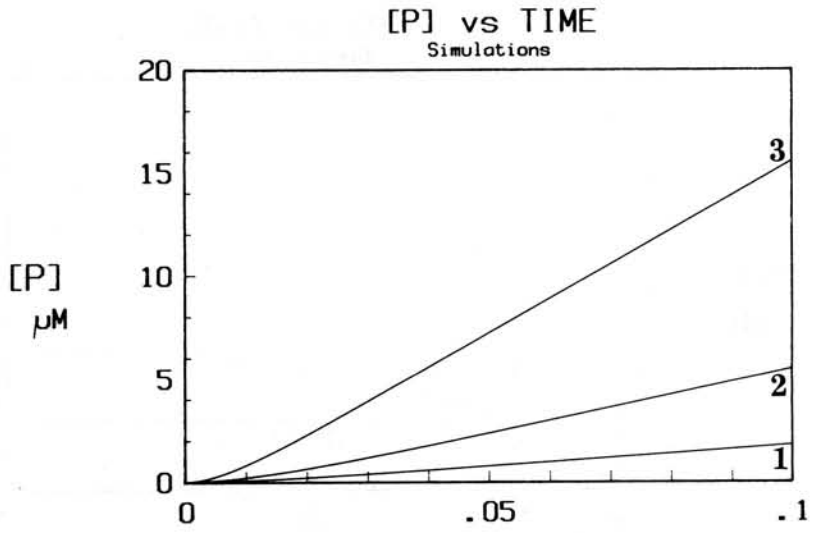

Figure 18-15

Constant	*Curve 1*	*Curve 2*	*Curve 3*
k_1	50	50	50
k_2	20	20	50
k_3	3	10	50

Other conditions are the same as in Fig. 18-14.

Figure 18-15 illustrates that under conditions where the concentration of P alone can be followed, there is a lag (as expected, since EP must be produced first) and that in the situation shown in Fig. 18-15, the production of P at its steady-state rate is attained after 20 to 30 ms. As expected, the intercept on the time axis $[= 1/(k_1 + k_2 + k_3)]$ can be affected by any of the three rate constants.

If the linear region is extrapolated to P = 0, the intercept is given by

$$0 = \frac{k_1 k_3 \mathrm{ET}}{k_1 + k_2 + k_3} t - \frac{k_1 k_3 \mathrm{ET}}{(k_1 + k_2 + k_3)^2} \tag{18-39}$$

and $t = 1/(k_1 + k_2 + k_3)$.

This formulation is of use if (and only if) one can measure P alone. However if, as is usually the case, the sum of EP + P is measured experimentally, we get, from Eqs. (18-34) and (18-35),

$$[\mathrm{EP}] + [\mathrm{P}] = \frac{k_1 k_3 \mathrm{ET}}{k_1 + k_2 + k_3} t + \frac{k_2 \mathrm{ET}}{k_1 + k_2 + k_3} - \frac{k_2 k_3 \mathrm{ET}}{(k_1 + k_2 + k_3)^2}(1 - e^{-(k_1 + k_2 + k_3)t}) \tag{18-40}$$

When t is large, the exponential term is negligible and the equation is linear in t.

$$\begin{aligned}[\mathrm{EP}] + [\mathrm{P}] &= \frac{k_1 k_3 \mathrm{ET}}{k_1 + k_2 + k_3} t + \left[\frac{k_1 \mathrm{ET}}{k_1 + k_2 + k_3} - \frac{k_1 k_3 \mathrm{ET}}{(k_1 + k_2 + k_3)^2}\right] \\ &= \frac{k_1 k_3 \mathrm{ET}}{k_1 + k_2 + k_3} t + \frac{(k_1 + k_2) k_1 \mathrm{ET}}{(k_1 + k_2 + k_3)^2}\end{aligned} \tag{18-41}$$

Hence the slope of a plot of ([EP] + [P]) versus t at large t is the steady-state rate, $k_1k_3\text{ET}/(k_1 + k_2 + k_3)$. Such plots are given in Fig. 18-16.

Several points can be made based on the simulated curves of Fig. 18-16. The steady-state rate of the reaction measured on a macroscopic time scale is not reached for 50 to 60 ms, and as expected from Fig. 18-14, the rate constant k_2 has a major effect on the rate at which the final steady-state rate is attained. In all the cases shown in Fig. 18-16A, a burst is observed: The rate of product release, k_3, is much smaller than the rate of initial product formation, k_1; also, the size of the burst is *not* stoichiometric with the active-site concentration in these cases. Figure 18-16B shows that a burst can be obtained even though the rate of initial product formation in EP, k_1, is equal to the rate of product release, k_3, although the burst size is diminished under such conditions. In curve 3 of part (B) where k_1 is truly rate limiting ($k_1 = k_3/100$), a linear ([EP] + [P]) versus time plot is observed. The reaction rate is governed solely by the rate of production of P in the EP complex, and the reaction is a true rapid equilibrium.

The intercept of such plots, by extrapolation of the linear part of the plot to $t = 0$, is

$$\text{intercept} = \frac{(k_1 + k_2)k_1\text{ET}}{(k_1 + k_2 + k_3)^2} \tag{18-42}$$

The relationship of the burst size to various rate constants is illustrated in Fig. 18-17. This figure shows the effects of the magnitude of k_1 compared to k_2 and k_3 on the size of the burst phase. As k_1 approaches the situation where $k_1 \gg k_2 + k_3$, the burst size nears the stoichiometric concentration of the active sites. Despite the fact that all three curves have the same k_3, the steady-state rate (attained within 50 ms) is different for all three. k_3 does not dominate the steady-state rate unless k_1 is at least $5 \times k_3$.

When $k_1 \gg k_2 + k_3$ this expression reduces to ET, and as before under this condition, the burst size is equal to the total enzyme active-site concentration. Without this restriction, however, the intercept *is not* the steady-state concentration of EP. The steady-state concentration is $k_1\text{ET}/(k_1 + k_2 + k_3)$. The intercept from the plot of ([EP] + [P]) versus t is, however, the steady-state concentration of EP multiplied by the factor $(k_1 + k_2)/(k_1 + k_2 + k_3)$, as indicated by

$$\text{intercept} = \frac{(k_1 + k_2)k_1\text{ET}}{(k_1 + k_2 + k_3)^2} = \frac{k_1\text{ET}}{k_1 + k_2 + k_3}\frac{k_1 + k_2}{k_1 + k_2 + k_3} \tag{18-43}$$

Thus, depending on the magnitude of k_3 relative to k_1 and k_2, the intercept (the apparent burst size) is *smaller* than the steady-state concentration of EP. The complete equation may be written as

$$([\text{EP}] + [\text{P}]) = At + B(1 - e^{-k_{\text{obs}}t}) \tag{18-44}$$

where A and B are obtained from the slope and intercept of the *linear* region of (EP + P) versus t, and $k_{\text{obs}} = k_1 + k_2 + k_3$.

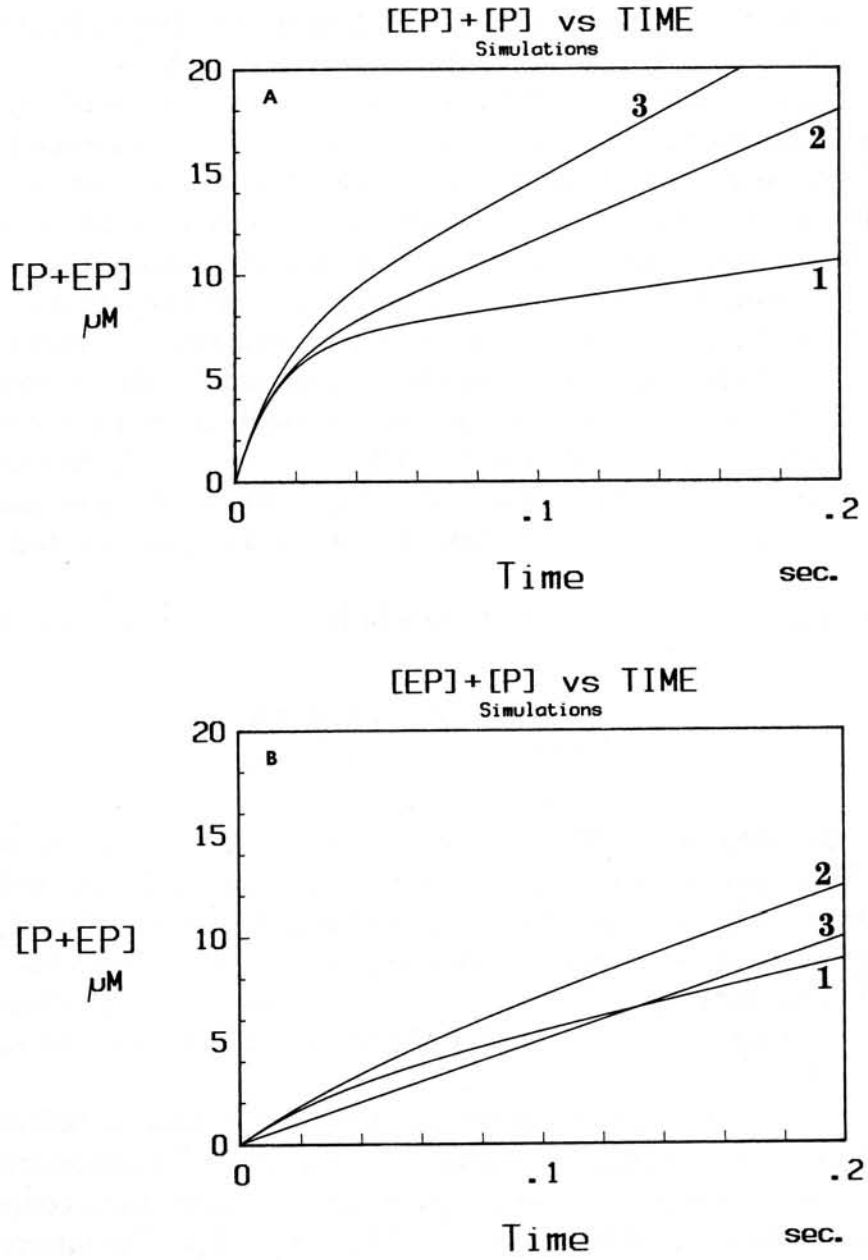

Figure 18-16 Computer simulations of ([EP] + [P]) versus time curves. k_1 is the rate constant for ES → EP, k_2 is the rate constant for EP → ES, and k_3 is the rate constant for product release, EP → E + P.

	Constant	*Curve 1*	*Curve 2*	*Curve 3*
(A)	k_1	50	50	50
	k_2	20	20	3
	k_3	3	10	10
(B)	k_1	10	10	10
	k_2	10	0.1	1000
	k_3	10	10	1000

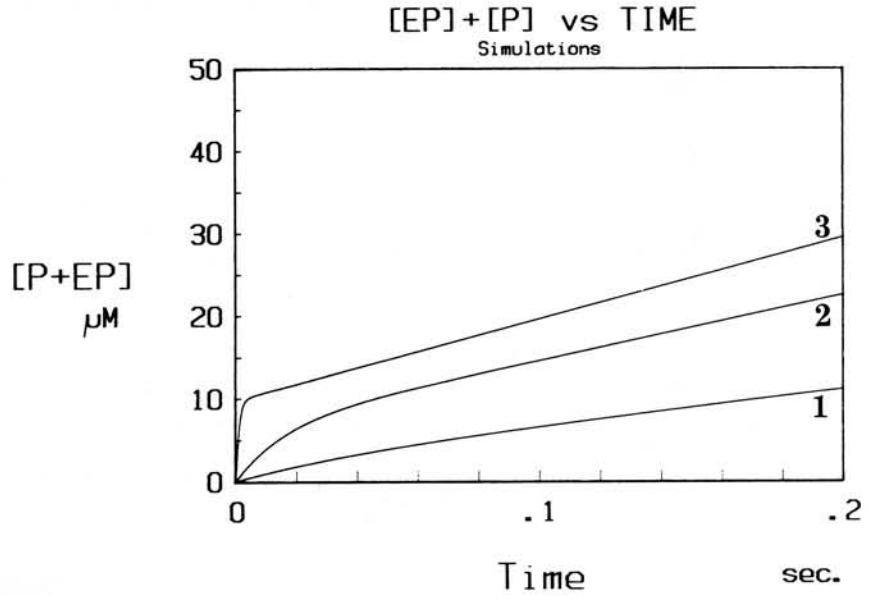

Figure 18-17 Rate constants are the same as in Fig. 18-16. Saturating concentrations of substrate are assumed. The active-site concentration is 10 μM.

Constant	*Curve 1*	*Curve 2*	*Curve 3*
k_1	10	50	1000
k_2	3	3	3
k_3	10	10	10

From this known value of A, At can be calculated during the exponential phase and subtracted to give the true exponential.

$$([\mathrm{EP}] + [\mathrm{P}]) - At = B(1 - e^{-k_{\mathrm{obs}}t}) \tag{18-45}$$

From Eq. (18-45) we get

$$[([\mathrm{EP}] + [\mathrm{P}]) - At] - B = -Be^{-k_{\mathrm{obs}}t} \tag{18-46}$$

Therefore,

$$\log \{B - [([\mathrm{EP}] + [\mathrm{P}]) - At]\} = \log B - \frac{k_{\mathrm{obs}}}{2.3} t \tag{18-47}$$

or

$$\log \{B + At - ([\mathrm{EP}] + [\mathrm{P}])\} = \log B - \frac{k_{\mathrm{obs}}}{2.3} t \tag{18-48}$$

In other words, since $B + At$ is the calculated OD obtained by extrapolation of the steady-state phase of the reaction to $t = 0$ (i.e., to B) and ([EP] + [P]) is obtained from the observed OD we can rewrite Eq. (18-48) as

$$\log (\mathrm{OD}_t^{\mathrm{calc}} - \mathrm{OD}_t^{\mathrm{obs}}) = \log \mathrm{OD}_{t_0}^{\mathrm{calc}} - \frac{k}{2.3} t \tag{18-49}$$

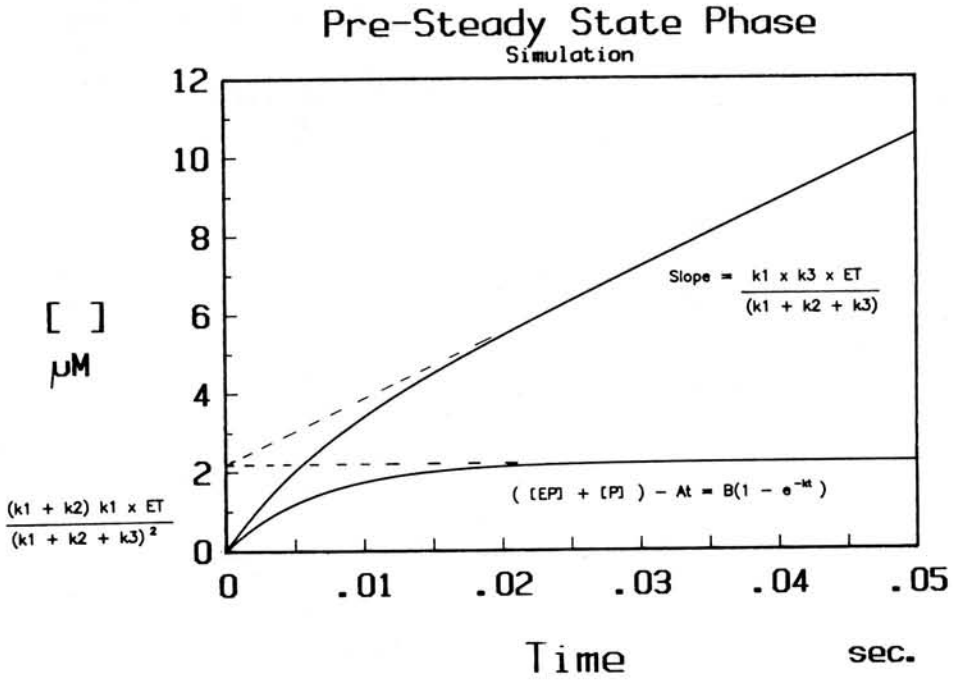

Figure 18-18 Computer simulation of ([EP] + [P]) versus time course (curve 1) and calculated exponential curve for the burst phase of the reaction. k_1 (=50) is the rate constant for ES → EP, k_2 (=50) is the rate constant for EP → ES, and k_3 is the rate constant for product release, EP → E + P. Saturating concentrations are assumed. The active-site concentration is 10 μM.

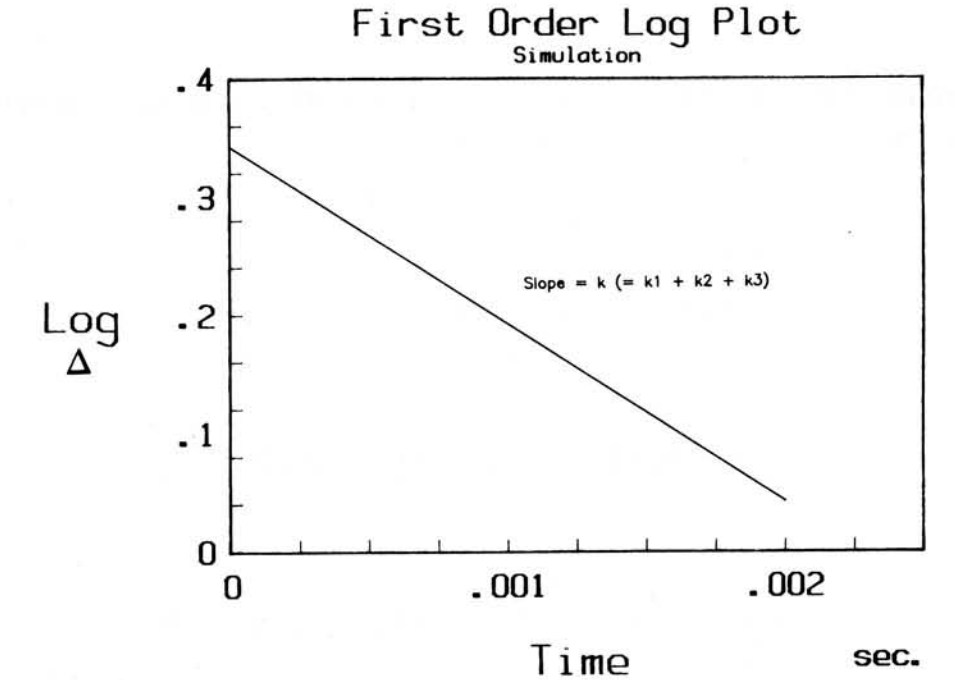

Figure 18-19 Plot of log ($OD_t^{calc} - OD_t^{obs}$) versus t. The former is the difference between the observed concentration of products and the concentration calculated by extrapolation of the steady-state rate to $t = 0$ in Fig. 18-18. The slope of the line is $-k_{obs}$, where k_{obs} is the rate constant of the exponential phase of the reaction (the burst rate). $k_{obs} = k_1 + k_2 + k_3$.

and from a plot of $\log(OD_t^{calc} - OD_t^{obs})$ versus t we get a value for k_{obs}, as shown in Figs. 18-18 and 18-19.

It is apparent that the quantities obtained from experimental (EP + P) versus t curves are (1) the *apparent* burst size (B) from extrapolation of the linear region to $t = 0$; (2) the slope, A, of the linear part of the curve, $k_1k_3ET/(k_1 + k_2 + k_3)$; and (3) $k_{obs} = k_1 + k_2 + k_3$ from the exponential phase of the curve. As a result, summarized in Fig. 18-19, we can calculate the true steady-state concentration of EP from the apparent burst size (B), A, and k_{obs}.

$$[EP] = \frac{B - A}{k_{obs}} \tag{18-50}$$

From points 2 and 3 we can calculate k_1k_3ET and (since ET is a known parameter) k_1k_3.

$$k_1k_3ET = Ak_{obs} \tag{18-51}$$

which also gives us k_3 as a function of k_1, and since $k_{obs} = k_1 + k_2 + k_3$ we obtain relative values of k_1 and k_2. From the ([EP] + [P]) versus t curve it is possible to separate [P] versus t or [EP] versus t time courses for the reaction (Fig. 18-20).

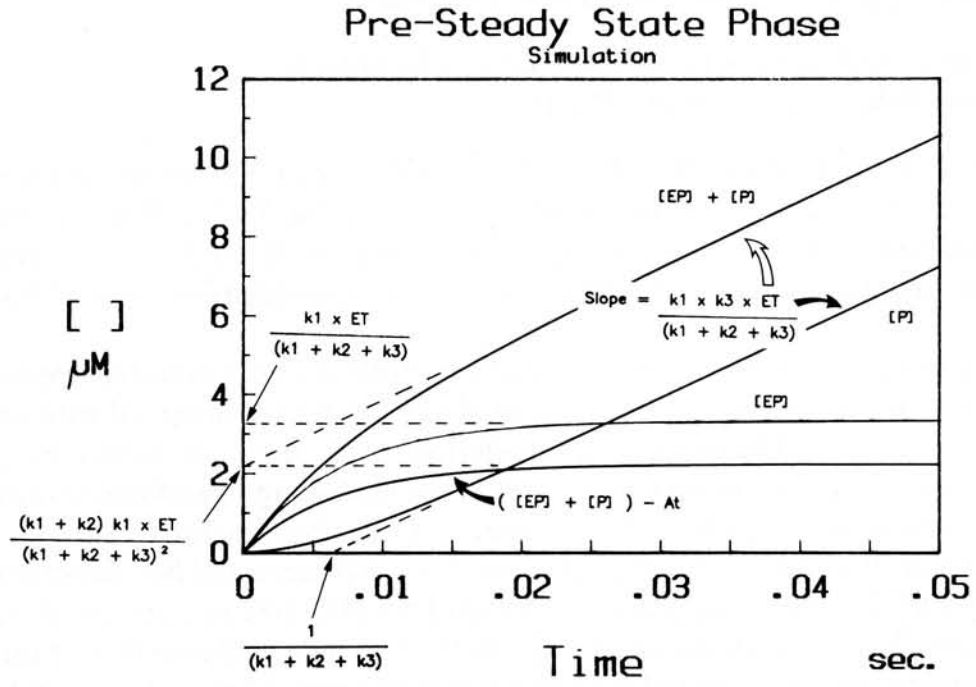

Figure 18-20 Summary of pre-steady-state phase for a reaction ES ↔ EP → E + P. Rate constants are the same as in Fig. 18-19. The intercept of the [P] versus t plot is $1/(k_1 + k_2 + k_3)$, and is the reciprocal of the rate constant, k_{obs}, of the burst phase. $k_{obs} = k_1 + k_2 + k_3$. If free product can be monitored, this gives an alternative method to that outlined in Figs. 18-18 and 18-19 to obtain a value for k_{obs}.

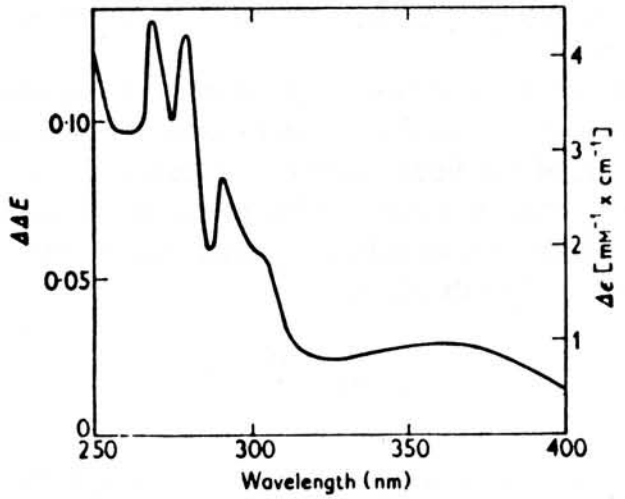

Figure 18-21 Difference spectrum of the complex of yeast GA-3P-DH with NAD at pH 8.0 and 20°C. Difference spectra measured at various concentrations of NAD between 0.02 and 1.00 m*M* were evaluated at various wavelengths to determine the apparent dissociation constant $K = 1.0 \times 10^{-5}$ and to extrapolate the measurements to 100% saturation. (Reprinted with permission from K. Kirschner, E. Gallego, I. Schuster, D. Goodall, *J. Mol. Biol.*, *58*, 29–50. Copyright 1971 Academic Press, Inc., New York.)

Examples of the Use of Rapid-Reaction Techniques

Cooperative Binding of NAD to Yeast Glyceraldehyde-3-Phosphate Dehydrogenase (GA-3P-DH)

When NAD binds to GA-3P-DH an absorbance at 360 nm specific for the coenzyme bound to the enzyme is formed, as shown in Fig. 18-21. This difference spectrum has been used to study the equilibrium binding of NAD to the enzyme and serves as a convenient spectral signal to follow in rapid-reaction studies of coenzyme binding.

In a temperature-jump study, relaxation processes were detected spectrophotometrically only in mixtures of enzyme and NAD; three were observed with relaxation times τ_1, τ_2, and τ_3. The processes characterized by τ_1 and τ_2 are both clearly second order, as evidenced by an increase of rate with increasing ligand concentration. At low concentrations $1/\tau_1$ and $1/\tau_2$ are separated only by a factor of 2 to 3.

The rate of the slow relaxation process, $1/\tau_3$, was measured by temperature jump at low [NAD] and by stopped flow at high [NAD]. $1/\tau_3$ is constant at very high ligand concentrations, as shown in Fig. 18-22. The independence of $1/\tau_3$ on enzyme concentration was extended to low NAD concentrations. Clearly, $1/\tau_3$ must be identified with a slow first-order process involving the enzyme–NAD complex.

The first relaxation process can be identified unequivocally with a second-order reaction,

$$\mathrm{E} + \mathrm{NAD} \underset{k_2}{\overset{k_1}{\rightleftharpoons}} \mathrm{E} \cdot \mathrm{NAD}$$

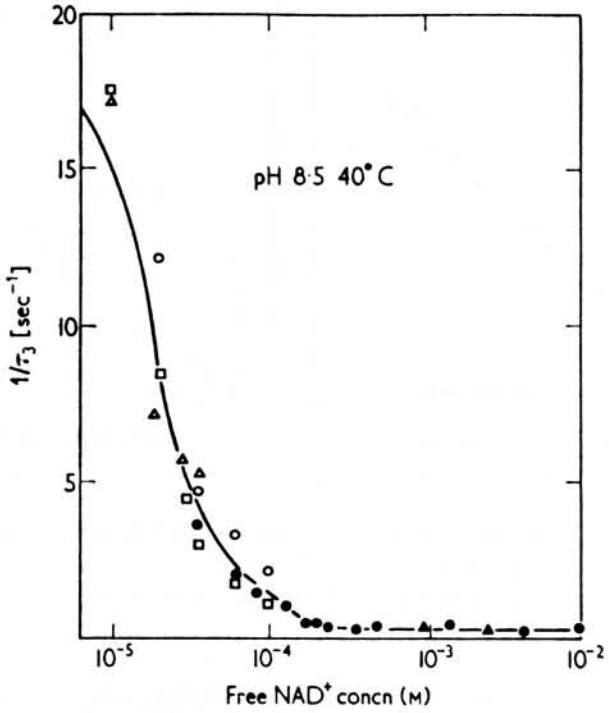

Figure 18-22 Dependence of $1/\tau_3$ on [NAD]. (Reprinted with permission from K. Kirschner, E. Gallego, I. Schuster, and D. Goodall, *J. Mol. Biol.*, *58*, 29–50. Copyright 1971 Academic Press, Inc., New York.)

Since it is well separated from the following step at high NAD concentrations, it can be regarded as an isolated process. The concentration dependence can thus be evaluated on the basis of

$$\frac{1}{\tau_1} = k_2 + k_1(\mathrm{E} + \mathrm{NAD}) \tag{18-52}$$

and at high concentrations of ligand the concentration of free binding sites ($\bar{\mathrm{E}}$) becomes negligible and Eq. (18-52) is reduced to

$$\frac{1}{\tau_1} = k_2 + k_1(\mathrm{NAD}) \tag{18-53}$$

From plots of $1/\tau_1$ versus NAD, as in Fig. 18-23, an estimate of the thermodynamic binding constant, $K_d = k_2/k_1 = 8 \times 10^{-5}\ M$, is obtained. This is smaller than the concentration of free NAD at half-saturation of approximately $2.2 \times 10^{-4}\ M$ (from direct binding studies), and thus the binding site involved in the fast relaxation process can be identified as a high-affinity site. The fact that the reciprocal relaxation time is an almost linear function of free NAD down to 3% saturation suggests that the concentration of free binding sites possessing high affinity are, under all conditions, small compared to the concentration of free NAD.

The second relaxation process is also clearly of second order. However, it can no longer be considered in isolation because it must be coupled to the faster process.

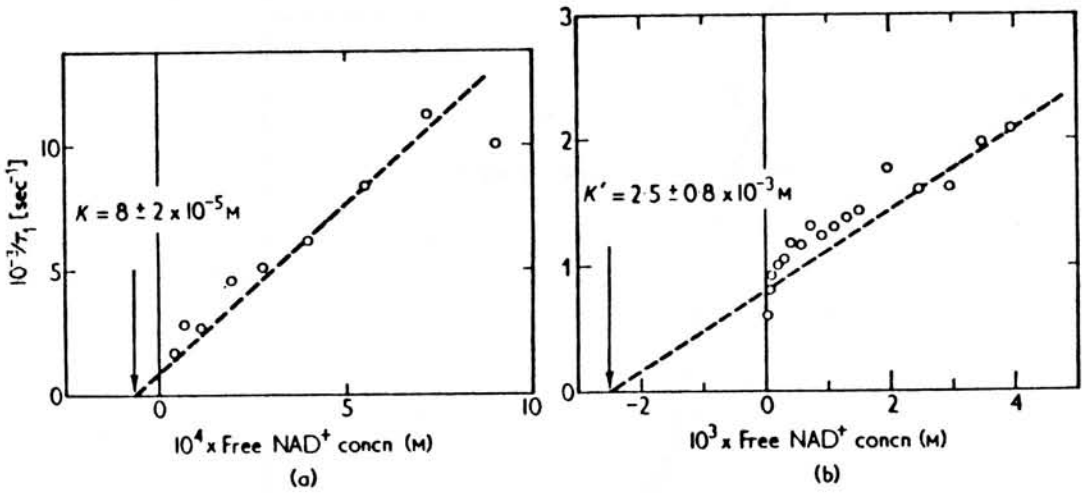

Figure 18-23 Dependence of $1/\tau_1$ and $1/\tau_2$ on the free [NAD]. (Reprinted with permission from: K. Kirschner, E. Gallego, I. Schuster, and D. Goodall, *J. Mol. Biol.*, *58*, 29–50. Copyright 1971 Academic Press, Inc., New York.)

If the binding sites exist independently, coupling is brought about by the common ligand (i.e., NAD), and the two reactions can be written as

$$\mathrm{E} + \mathrm{NAD} \underset{k_2}{\overset{k_1}{\rightleftharpoons}} \mathrm{E} \cdot \mathrm{NAD} \qquad \text{fast } (\tau_1)$$

and

$$\mathrm{E}' + \mathrm{NAD} \underset{k_2'}{\overset{k_1'}{\rightleftharpoons}} \mathrm{E}' \cdot \mathrm{NAD} \qquad \text{slow } (\tau_2)$$

Coupling can also occur via a common enzyme species, leading to the compulsory order of addition of ligands.

$$\mathrm{NAD} + \mathrm{E} + \mathrm{NAD} \longleftrightarrow \mathrm{NAD} \cdot \mathrm{E} + \mathrm{NAD} \longleftrightarrow \mathrm{NAD} \cdot \mathrm{E}' + \mathrm{NAD} \longleftrightarrow \mathrm{NAD} \cdot \mathrm{E}' \cdot \mathrm{NAD}$$

The two different types of binding sites are symbolized by differentiating between the left- and right-hand sides of E. Some unspecified isomerization of NAD · E to NAD · E′ is required to generate the second binding site.

In attempting to explain only two binding reactions in the millisecond time range, the isomerization must necessarily have a comparable rate, and one of the intermediates (e.g., NAD · E′) must be present at an undetectable concentration.

The compulsory-order addition mechanism is unnecessarily complex and neglects the fact that the *only* first-order process observed is slow compared to the binding steps. The data thus favor the independent-binding-sites scheme. In this case, the second relaxation process would obey the relation shown by

$$\frac{1}{\tau_2} = k_2' + k_1' \left(\bar{\mathrm{D}} + \bar{\mathrm{E}} \frac{K + \bar{\mathrm{D}}}{K + \bar{\mathrm{D}} + \bar{\mathrm{E}}} \right) \tag{18-54}$$

where $\bar{\mathrm{D}}$ is the concentration of free NAD.

At a high concentrations of NAD (i.e., $\bar{D} > \bar{E}, \bar{E}'$), decoupling of the two binding reactions occurs, reducing Eq. (18-54) to

$$\frac{1}{\tau_2} = k'_2 + k'_1(\bar{D}) \tag{18-55}$$

The limiting slope of the values of $1/\tau_2$ at high NAD concentrations can now be used to obtain a rough estimate of the pertinent dissociation constant, $K'_d = 2.5 \times 10^{-3}\ M$, which is far greater than the concentration of free NAD at half-saturation, and thus the binding site can be characterized as a low-affinity binding site.

Significance of Relaxation Times to Allosteric Models

The simplest sequential mechanism of Koshland, Nemethy, and Filmer, and the concerted mechanism of Monod et al., can be distinguished in favorable cases by such studies.

The sequential mechanism illustrated in Fig. 18-24 is characterized by five conformational hybrids of the enzyme, which are interrelated by four consecutive binding reactions. The implications for the relaxation kinetics of such a system are that only the superposition of second-order processes (a maximum of four) can be observed. Although the progressive changes of affinity could be due to induced conformational changes, the simplifying assumption converts the sequences of binding followed by a conformational change into an overall binding process. That is, isomerizations do not occur as independently observable elementary steps. It is clear that the simplest sequential mechanism cannot account for the existence of τ_3, no matter what the values of the individual rate and equilibrium constants are.

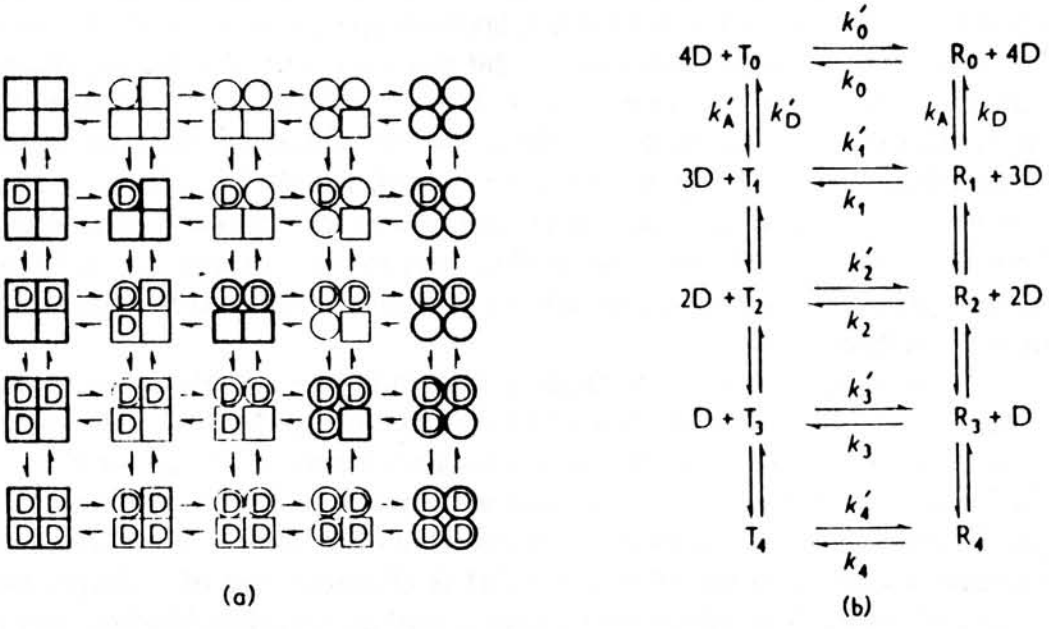

Figure 18-24 Sequential and concerted allosteric models for ligand binding cooperativity. (Reprinted with permission from K. Kirschner, E. Gallego, I. Schuster, D. Goodall, *J. Mol. Biol.*, *58*, 29–50. Copyright 1971 Academic Press, Inc., New York.)

The concerted mechanism, however, explicitly allows independent isomerization reactions. For a tetrameric enzyme this mechanism is characterized by nine relaxation times. In the special case where isomerization is much slower than binding, and where the rates of binding are sufficiently separated, it is possible to derive closed analytical expressions for all nine relaxation times.

To the extent that the condition of identity and independence of the binding sites within each one of the two states is fulfilled, six out of nine relaxation processes have zero amplitudes. This degeneracy results from the fact that the only physical process associated with a finite enthalpy change is the binding of the ligand to the active site in either the *R* or the *T* state. The remaining relaxation times are related to normal modes involving the redistribution of ligand between equivalent binding sites at constant ligand concentration. These processes have zero enthalpy changes by definition. Under such conditions only three relaxation times are detectable, two of which show a dependence on ligand concentration while the third is independent of the ligand concentration. In the case of NAD binding to yeast GA-3P-DH, the observed results are consistent with a concerted model.

Binding of NADH to Yeast Glyceraldehyde-3-Phosphate Dehydrogenase

NADH, on binding to the enzyme, quenches protein fluorescence ($_{290}F_{350}$) and also shows an increase in the polarization of the reduced nicotinamide fluorescence ($_{340}F_{450}$). Either of these parameters can be used to study NADH binding to the enzyme, in addition to monitoring changes in the NADH fluorescence upon binding. In rapid-reaction studies only one relaxation process was detected in mixtures of enzyme and NADH in the range $\tau = 10\ \mu s$ to 500 ms. Neither the apoenzyme nor the NADH solution showed measurable relaxation spectra when studied separately.

The characteristic relaxation time τ_1 did not vary with the specific method of observation: Protein fluorescence excited at 290 nm and measured between 300 and 400 nm, NADH fluorescence excited at 290 or 340 nm and observed at above 400 nm, or the polarization of NADH fluorescence excited at 340 nm. In each case the temperature jump resulted in rapid initial changes in the observed parameters that could not be resolved within the time resolution of the instrument, $\tau_{min} = 10\ \mu s$, and are probably due to the intrinsic dependence of fluorescence quantum yield and polarization on temperature.

The observed signs of the amplitudes corresponding to the subsequent relaxation process are in the direction of increasing dissociation of NADH with increasing temperature, as predicted from equilibrium measurements at 20 and 40°C.

The relaxation experiments were done with two different total enzyme concentrations (20 and 0.2 mg/ml) and various methods of observation. An increase of $1/\tau_1$ with increasing concentration of free NADH is characteristic of a simple binding process at each of the four apparently identical and independent binding sites of the tetrameric enzyme.

The data obtained (see Fig. 18-25) for the lower enzyme concentration obey a linear relationship down to very low concentrations of NADH. At higher enzyme concentrations $1/\tau_1$ deviates at low concentrations of NADH. At the high NADH

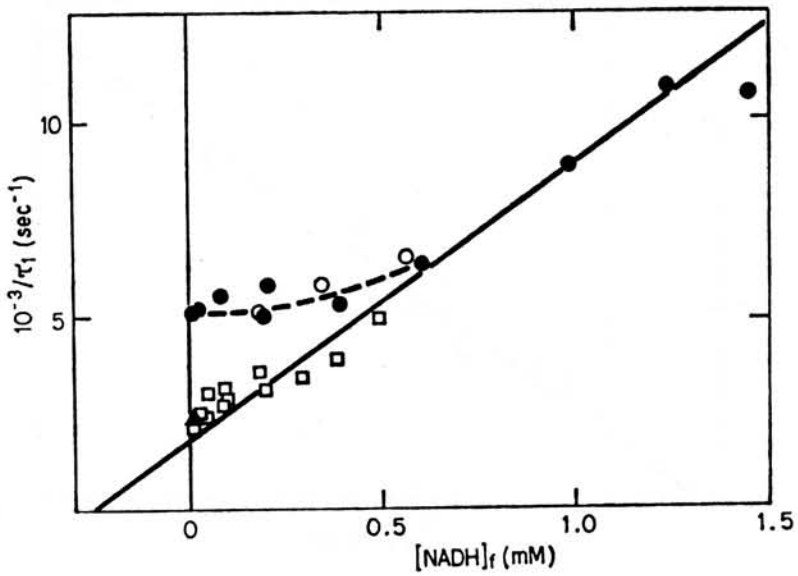

Figure 18-25 Dependence of $1/\tau_1$ on free [NADH] for NADH binding to yeast GA-3P-DH. [Reprinted with permission from: G. von Ellenrieder, K. Kirschner, and I. Schuster, *Eur. J. Biochem.*, *26*, 220–236 (1972).]

concentrations it merges into the straight line extrapolated from the measurements at low enzyme concentration.

This behavior is that expected for a simple binding reaction where the reciprocal relaxation time $1/\tau_1$ is related to the equilibrium concentrations of free binding sites ($\bar{E}$) and free NADH ($\overline{NADH}$) by the expression given in

$$\frac{1}{\tau_1} = k_2 + k_1(\bar{E} + \overline{NADH}) \tag{18-56}$$

For $\overline{NADH} \gg \bar{E}$, $1/\tau_1$ is nearly related to $\overline{NADH}$. An upward deviation of $1/\tau_1$ with decreasing concentration of $\overline{NADH}$ is to be expected only when $\bar{E}$ and $\overline{NADH}$ are comparable (i.e., at a high level of total enzyme concentration).

When the data are plotted in the form $1/\tau_1$ versus $\bar{E} + \overline{NADH}$, a strictly linear plot is obtained at both enzyme concentrations, as seen in Fig. 18-26. The values of k_2 and k_1 obtained from the intercept and slope, respectively, of such a plot are $k_2 = 1.9 \times 10^{-3}\ s^{-1}$ and $k_1 = 7.9 \times 10^6\ M^{-1}\ s^{-1}$. Within the error limits, the value of the thermodynamic dissociation constant, $k_d = k_2/k_1 = 0.24$ mM, agrees well with the value of 0.2 mM obtained from direct binding studies by gel filtration.

Multiple Turnover Studies of the Reaction Catalyzed by Glutamate Dehydrogenase

Glutamate dehydrogenase catalyzes the reversible oxidative deamination of glutamate. The reductive reaction, using NADH as coenzyme, is conveniently monitored by following absorbance at 340 nm. When enzyme is rapidly mixed with NADH, 2-oxoglutarate, and ammonia, no evidence of a pre-steady-state burst is seen (Fig. 18-27), consistent with the proposed rapid-equilibrium random-order addition of substrates in the reductive amination reaction.

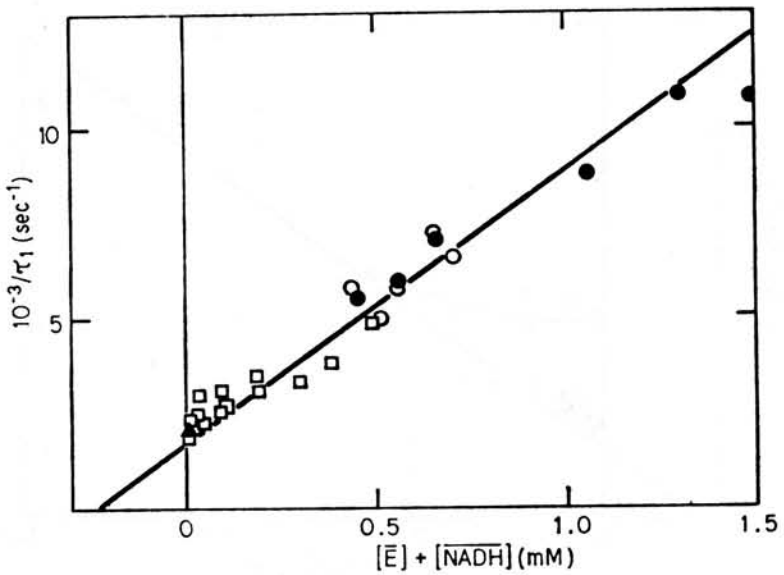

Figure 18-26 Dependence of $1/\tau_1$ on ([E] + [NADH]) for NADH binding to yeast GA-3P-DH. [Reprinted with permission from: G. von Ellenrieder, K. Kirschner, and I. Schuster, *Eur. J. Biochem.*, *26*, 220–236 (1972).]

When the oxidative deamination reaction is monitored at pH 8.0 with varying amounts of glutamate, a distinct burst phase is seen at 10 m*M* glutamate and 250 μM NAD or NADP, as shown in Fig. 18-28. As indicated, three parameters—the steady-state rate, the burst size, and the burst rate—are obtained from such data. The existence of the burst clearly indicates that under these conditions a product release step is the overall rate-limiting step. The burst size, as discussed earlier, is less than the steady-state concentration of the enzyme–product complex, and in this instance

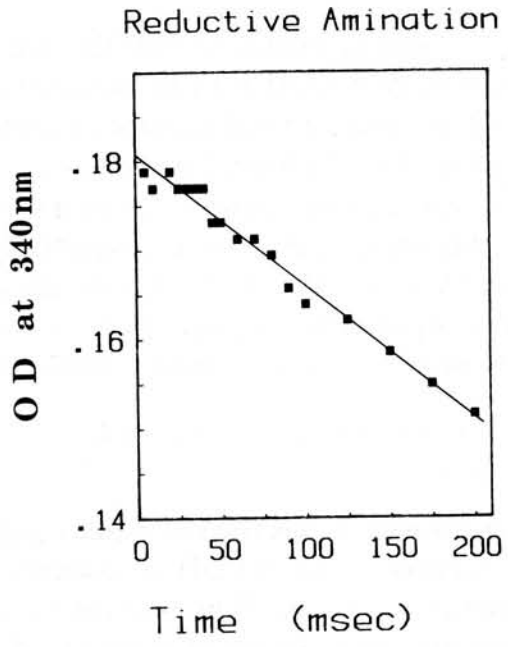

Figure 18-27 Results of stopped-flow study of the reductive amination reaction catalyzed by glutamate dehydrogenase.

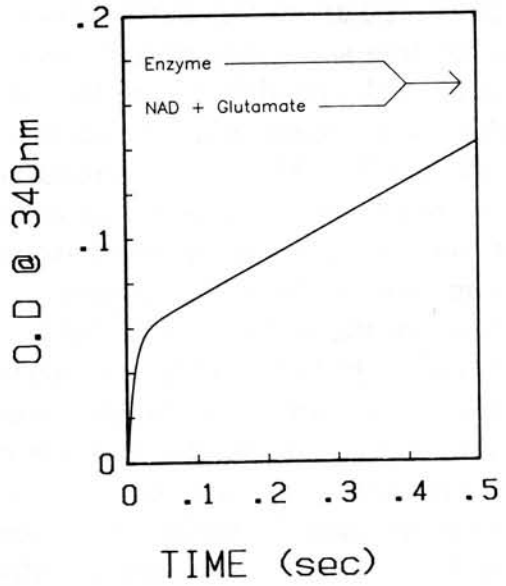

Figure 18-28 Oxidative deamination of glutamate dehydrogenase at pH 8.0 with 10 mM glutamate and 250 μM NAD.

is less than half the total active-site concentration. When the glutamate concentration is raised, a number of changes occur in the observed results: The steady-state rate decreases above 50 mM glutamate, the burst size approximately doubles, and as shown in Fig. 18-29, a distinct lag phase is observed between the pre-steady-state burst and the steady-state production of NADH.

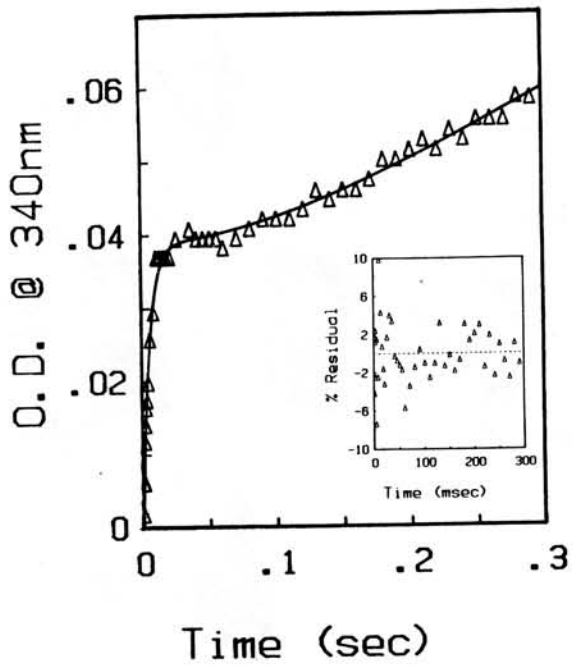

Figure 18-29 Oxidative deamination of glutamate dehydrogenase at high glutamate concentrations. The solid line is a best fit of the data to Eq. (18-57), and the insert is a residuals plot of the fit.

Time-difference spectral studies of the burst phase, the lag phase, and the steady-state phase of the reaction show that during the burst an enzyme–NADH-2-oxoglutarate complex is formed, and that during the lag phase 2-oxoglutarate is slowly released, presumably as the result of a rate-limiting conformational change, while, as would be expected, free NADH is rapidly produced during the steady-state phase. The doubling of the burst size, the appearance of the lag at high glutamate, and the apparent substrate inhibition seen in the steady-state rate led to the postulate of a reciprocating subunit mechanism for this hexameric enzyme. At low glutamate concentrations three or fewer of the subunits bind NAD and glutamate and react to produce NADH and 2-oxoglutarate bound to the enzyme. NAD and glutamate bind to the three vacant sites per hexamer and induce a conformational change that causes the release of NADH and 2-oxoglutarate from the original three sites. This process is repeated in a reciprocating subunit manner, with the two halves of the hexamer alternating in the production of NADH and 2-oxoglutarate. At high glutamate concentrations more than three sites are initially filled with NAD and glutamate and react to give NADH and 2-oxoglutarate and, as observed, the burst size increases. However, at this point there are essentially no empty sites for NAD and glutamate to bind to, so that product release is enhanced. As a result, there is a very slow release of 2-oxoglutarate, leading to the observed lag phase. Once 2-oxoglutarate has been released from a sufficient number of sites, glutamate can bind and reciprocation take place, leading to the steady-state rate of product accumulation. This model is shown in Fig. 18-30 and is described by

$$P_{\text{total}} = A(1 - e^{-kt} + mt(1 - e^{-lt})) \tag{18-57}$$

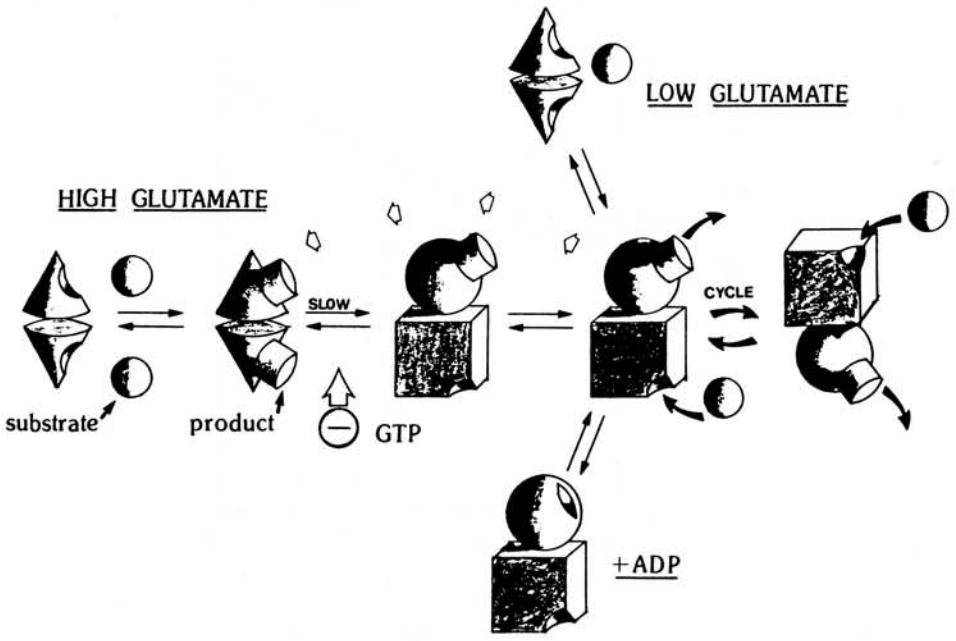

Figure 18-30 Model for the reciprocating subunit mechanism of glutamate dehydrogenase proposed on the basis of stopped-flow studies.

where P_{total} is the total amount of product NADH (free or enzyme-bound) produced at any time t, A is the burst amplitude, k the burst rate, m the steady-state rate of NADH production, and l the rate constant of the rate-limiting conformational change that allows 2-oxoglutarate to be released from the enzyme in the absence of binding energy input from glutamate. When the enzyme is able to operate via a reciprocating subunit mechanism at low glutamate concentrations, the rate constant l is fast and no lag is observed. As shown in the insert in Fig. 18-29, Eq. (18-57) provides an excellent description of the experimental data obtained at high glutamate concentrations, providing support for the model shown in Fig. 18-30.

From these examples it is apparent that information from rapid-reaction studies is invaluable in studying ligand binding steps as well as the complete catalytic reaction. In particular, data from such studies have proved useful in discerning among various allosteric models that have been proposed and, as shown by the last example, have allowed more complex allosteric models to be explored.